APL Photonics

High-performance geometric phase elements in silica glass

Cite as: APL Photonics **2**, 066104 (2017); https://doi.org/10.1063/1.4984066
Submitted: 27 March 2017 • Accepted: 11 May 2017 • Published Online: 26 May 2017

Rokas Drevinskas and Peter G. Kazansky

High-performance geometric phase elements in silica glass

Rokas Drevinskas[a] and Peter G. Kazansky
Optoelectronics Research Centre, University of Southampton, Southampton SO17 1BJ, United Kingdom

(Received 27 March 2017; accepted 11 May 2017; published online 26 May 2017)

High-precision three-dimensional ultrafast laser direct nanostructuring of silica glass resulting in multi-layered space-variant dielectric metasurfaces embedded in volume is demonstrated. Continuous phase profiles of nearly any optical component are achieved solely by the means of geometric phase. Complex designs of half-wave retarders with 90% transmission at 532 nm and >95% transmission at >1 μm, including polarization gratings with efficiency nearing 90% and computer generated holograms with a phase gradient of ~0.8π rad/μm, were fabricated. A vortex half-wave retarder generating a single beam optical vortex with a tunable orbital angular momentum of up to $\pm 100\hbar$ is shown. The high damage threshold of silica elements enables the simultaneous optical manipulation of a large number of microobjects using high-power laser beams. Thus, the continuous control of torque without altering the intensity distribution was implemented in optical trapping demonstration with a total of 5 W average power, which is otherwise impossible with alternate beam shaping devices. In principle, the direct-write technique can be extended to any transparent material that supports laser assisted nanostructuring and can be effectively exploited for the integration of printed optics into multi-functional optoelectronic systems. [http://dx.doi.org/10.1063/1.4984066]

INTRODUCTION

Conventional optics manipulates the properties of light via an optical path difference by controlling the thickness or refractive index of the material. Despite decade-long expertise in the fabrication of optical components, precision and quality still remain a challenging problem. The recent advances in flat optics have challenged the limitations of conventional optics by implementing ultrathin planar elements that manipulate light waves via subwavelength-spaced phase shifters with spatially varying phase response.[1,2] Various phase profiles of nearly any optical components ranging from lenses, gratings, and vortex-phase plates to elements capable of bending the light in unusual ways have been demonstrated using plasmonic metasurfaces[3,4] or dielectric gradient metasurfaces[5–9] referred to as geometric phase (Pancharatnam-Berry phase[10–12]) optical elements and realized by space-variant polarization manipulations.[13]

One of the approaches for designing geometric phase elements is to exploit the transparent dielectrics which originate from birefringence. Thus, the desired phase pattern of the wave is directly encoded in the optical axis orientation and is equal to twice the rotation angle of the local retarder. However, despite the numerous techniques enabling the manufacturing of high-efficiency elements,[6,14–18] the limited technological flexibility and low material durability, e.g., liquid crystals with a damage threshold of 0.2 J/cm^2, prevent these elements from being widely integrated in consumer electronics or high-power laser applications. Here we propose a direct-write ultrafast laser nanostructuring of silica glass as an alternative method which is capable of fabricating geometric phase optics. The key advantage of using femtosecond pulses for direct laser writing, as opposed to longer pulses, is

[a]E-mail: R.Drevinskas@soton.ac.uk

that they can rapidly deposit energy in solids with high-precision. The light is absorbed, and the optical excitation ends before the surrounding lattice is perturbed, which results in highly localized nanostructuring without collateral material damage.[19,20]

A decade ago, the formation of self-organized subwavelength periodicity structures, referred to as nanogratings, in the bulk of silica glass after irradiation with ultrashort light pulses was observed.[21,22] Despite many hypotheses to explain the mechanism of the peculiar self-organization, the formation of the periodic nanostructures remains under debate giving the ideas of seeding processes governed by the randomly distributed inhomogeneity.[21,23–29] Recently it was demonstrated that these nanostructures are nanoporous planes filled with decomposed SiO_2 and oxygen.[30,31] Such a periodic assembly behaves as a uniaxial birefringent material with the optical axis oriented parallel to the polarization of incident laser beam. The birefringence value of these thermally stable nanostructures is negative ($\Delta n \approx -5 \times 10^{-3}$) and of the same order as the natural birefringence of uniaxial crystals such as quartz, ruby, and sapphire.[32] As a result, these modifications serve as a perfect candidate for designing phase optics. A number of optical elements including Fresnel zone plates,[33] dynamic phase holograms,[34–38] polarization diffraction gratings, and polarization converters[7,39–41] have been demonstrated. Despite the vast number of devices, the specifications have to be improved towards the practical applications. In this work, we leverage the potential implementations of silica nanogratings by achieving high performance geometric phase manipulating elements.

We fabricate complex designs of half-wave retarders with up to 90% transmission in the visible spectral range, polarization gratings with efficiencies as high as 90%, computer generated holograms with a phase gradient of ~0.8π rad/μm, and vortex retarders generating an orbital angular momentum of up to ±100$\hbar$. The highly durable silica nanostructures enable the demonstration of simultaneous optical manipulation of a large number of micro-objects using high-power laser beams.

RESULTS AND DISCUSSIONS

Typically, silica nanogratings with a periodicity of ~300 nm and duty cycle of roughly 10% of the nano-planes oriented perpendicular to the polarization are formed. The thickness of structures diverges from several microns to tens of microns depending on the numerical aperture of the objective used for printing. Then the retardance, also referred to as phase retardation, is defined as $\varphi = h(n_e - n_o)2\pi/\lambda = h\Delta n 2\pi/\lambda$, where h is the thickness, n_e, n_o—extraordinary and ordinary effective refractive indices, and λ is the probing wavelength. Thus, any phase retardation can be achieved by printing multilayered patterns in three-dimensions.

Local orientation of nanogratings, i.e., the azimuth of the slow-axis of laser induced form birefringence, $A(x, y)$ [Fig. 1(a)], were continuously controlled by rotating the half-wave plate, $\theta(x, y)$, mounted on the motorized rotational stage before the objective lens. The local azimuth of the slow-axis of an imprinted element is expressed as

$$A(x, y) = 2\theta(x, y) - \pi/2, \tag{1}$$

where the orientation of the half-wave plate corresponds to the orientation of the polarization of the incident linearly polarized laser beam used for silica modification, and the azimuth-offset of $\pi/2$ occurs due to the nanograting orientation, which is always perpendicular to the incident polarization. As a result, phase profiles of complex geometric phase (GP) elements were imprinted; and the circularly polarized light transmitted through the elements experiences the relative phase change equal to $\phi(x, y) = \pm 2A(x, y)$, where the sign is defined by the handedness of the input polarization.

The dispersion analysis performed in the spectral region from 440 nm to 680 nm revealed a chromatic behavior of the wave plates tuned for 532 nm [Fig. 1(b)]. The retardation value varies from 0.8π to π, and less than 5% variation in retardance is observed in the spectral region from 512 nm to 572 nm wavelength. The transmission coefficient at 532 nm, where the phase retardation is about 0.99π, is roughly of ~0.9 [Fig. 1(b)]. Despite the negligible linear absorption of silica, the transmission follows the $\sim\lambda^{-4}$ dependence, which is related to the scattering of the subwavelength

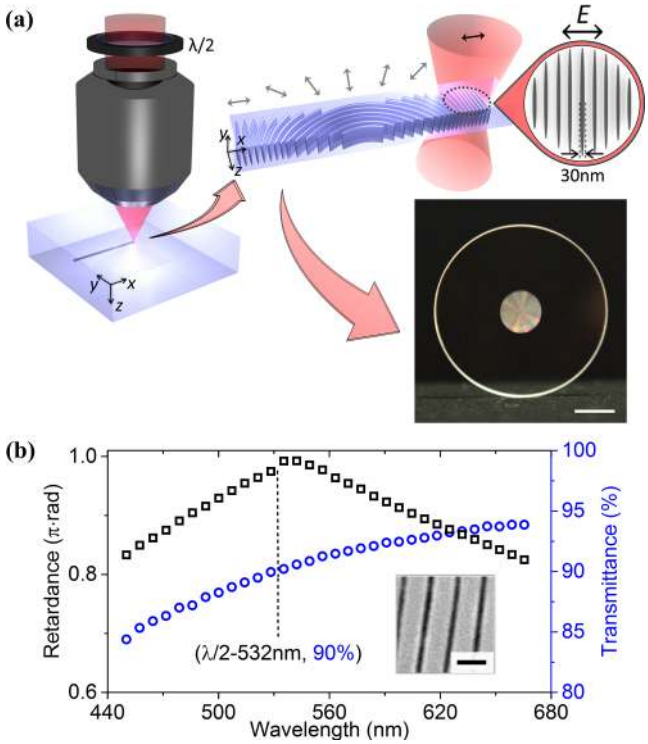

FIG. 1. Ultrafast laser nanostructuring of silica glass. (a) Graphical visualization of engineered anisotropy inside a slab of the transparent medium. Polarization of the incident laser beam (black arrows) is continuously controlled by the half-wave plate (λ/2) inserted before the objective. Azimuth of the slow-axis of induced form birefringence is always oriented parallel to nanograting. As a result, large-scale geometric phase optical elements are fabricated. Scale bar is 6 mm. (b) Phase retardation (□) and optical transmission (○) spectra of the imprinted half-wave retarder tuned for a 532 nm wavelength. Inset: electron microscopy generated image showing the characteristic topography of laser-induced nanogratings. Scale bar is 300 nm.

structure [Fig. 1(b), inset]. The higher transmission can be achieved at longer wavelengths where lower scattering is expected. This gives around 96% of transmission at 1064 nm.

When designing GP elements by laser direct writing, it is important to ensure the continuity of imprinted nanogratings. If the phase gradient is introduced, the local fields as well as the induced structures are perturbed by the previously printed structure. Thus, the induced retardance value drops with the increase of the azimuth density of slow-axis rotation [Fig. 2(a)]. The effect is strongly dependent on the focusing conditions. If the azimuth density increases up to 0.5 rad/μm, the average retardance value drops by 9.5× for 0.16 NA, 1.86× for 0.35 NA, 1.67× for 0.55 NA, and 1.75× for 1.2 NA (water immersion), with the corresponding increase in the relative standard deviation by 6 times, 2.8 times, 1.4 times, and 2.5 times, respectively. Even the energy control does not provide a way around this, as the retardance drops due to the material damage observed slightly above the pulse energies of 1.6 μJ for 0.16 NA, 0.8 μJ for 0.35 NA and 0.55 NA, and 0.4 μJ for 1.2 NA. This indicates that to achieve the target retardation, the thickness of the structures has to be increased. Therefore, for most of the experiments done in this work, a 0.55 NA objective lens in combination with a multilayer printing approach was implemented.

The azimuth density of the slow-axis rotation affects not only the retardance value but also the quality of the phase profile. Under the processing conditions reported in this work, the maximum achieved the azimuth density, which sufficiently follows the linear-phase profile, is roughly of 0.4π rad/μm [Fig. 2(b)]. This corresponds to the phase density of 0.8π rad/μm, which brings printed optics to the next level allowing high-density GP elements such as vortex retarders with a diameter of 10 mm generating optical vortices with a topological charge as high as 10 000.

The laser material processing conditions used to print GP elements were chosen to attain the maximum quality of structures, based on the experimental data from Figs. 1 and 2. The parameter window for laser-induced nanogratings is very large and is chosen for each application

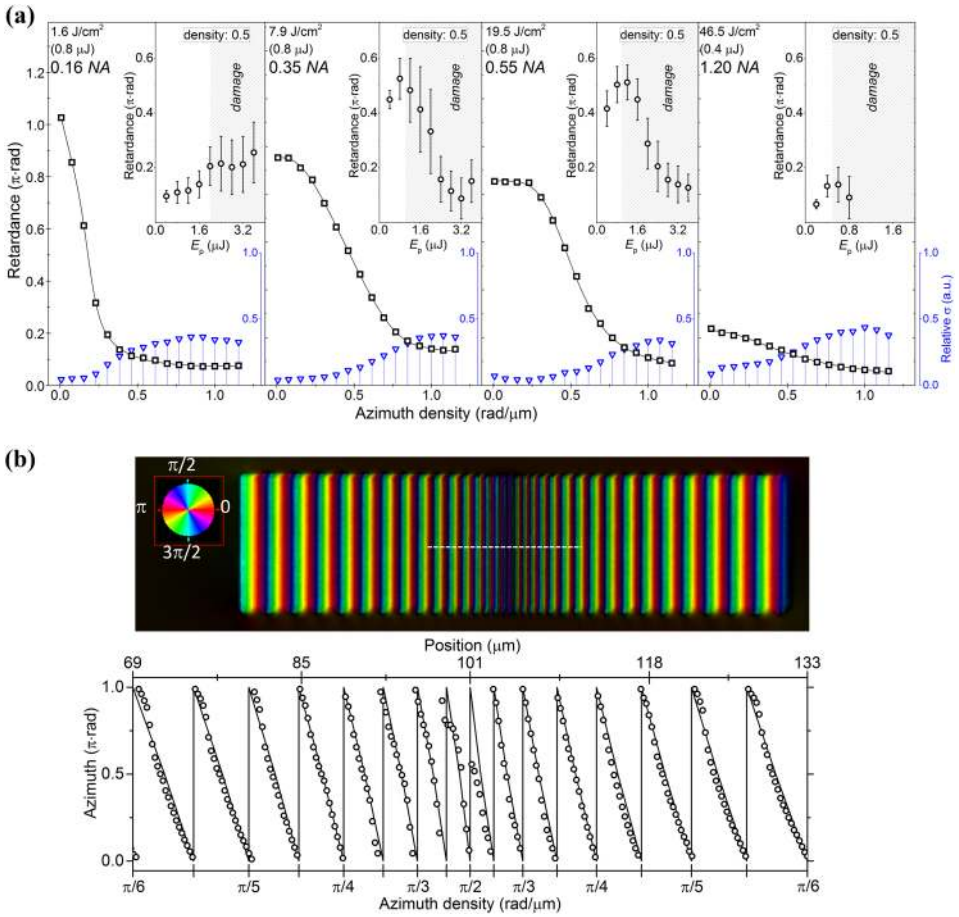

FIG. 2. (a) Induced phase retardation as a function of various processing conditions such as the azimuth density of the slow-axis rotation (□), pulse energy E_p (◊, insets), and numerical aperture (left to right: 0.16–1.2 NA). Blue open triangles (▽) show the relative standard deviation of the measured retardation value as a function of azimuth density of the slow-axis rotation. The azimuth density experiments were performed at a fixed pulse energy of 0.8 μJ for 0.16 NA, 0.35 NA, and 0.55 NA, and 0.4 μJ for 1.2 NA, and the pulse energy experiments were performed at a fixed azimuth density of 0.5 rad/μm. The retardance measurement system was operating at 546 nm wavelength. (b) Azimuth of the slow-axis of a laser induced form birefringence dependence on its rotation density. Top image—the azimuth of the slow-axis of the imprinted linear-phase element with the density varying from 0.05π rad/μm to 0.5π rad/μm; bottom graph—the profile (white dashed line in top image) of azimuth of the slow-axis extracted from the birefringence image. Pseudo colours (the inset in the top image) indicate the local orientation of the slow-axis. The birefringence measurement system was operating at 546 nm wavelength.

separately according to the target diameter, processing time, required azimuth density, and total losses.

The blazed polarization grating (PG) with the geometric phase varying in the x-direction as $\phi(x) = \pm A(x) = \pm (2\pi/a)x|_{\text{mod } 2\pi}$ was printed inside silica glass [Figs. 3(a) and 3(b)]. The periodicity of the PG was set to $a = 60$ μm. For an incident plane wave with the polarization state $|E_{in}\rangle$, the resulting field generated by the PG is $|E_{out}\rangle| = \eta_E |E_{in}\rangle + \eta_R e^{i2A(x,y)} |R\rangle + \eta_L e^{-i2A(x,y)} |L\rangle$,[42] where $\eta_E = 1/2(t_x + t_y e^{i\varphi})$, $\eta_R = 1/2\left(t_x - t_y e^{i\varphi}\right)\langle E_{in}|L\rangle$, and $\eta_L = 1/2\left(t_x - t_y e^{i\varphi}\right)\langle E_{in}|R\rangle$ are the complex field efficiencies with $\langle E_{in}|R, L\rangle$ as an inner product of the left-handed $|L\rangle$ and right-handed $|R\rangle$ circular polarizations, φ is the retardation of the imprinted element, and $t_{x,y}$ are the transmission coefficients for the light polarized perpendicular and parallel to the optical axis. The imprinted PG with $t_{x,y} \approx 0.9$ and $\varphi \approx 0.99\pi$ at a central wavelength of 532 nm [Fig. 1(b)] is expected to diffract around 0.9 of the total incident light intensity, while the remaining 0.1 would be scattered. Thus, the efficiency expressed as a ratio of first order diffracted light and total transmitted light, $\eta_{1st} = E_{1st}/E^{(T)}_{total}$, would be ~100%. However, the characterization of the imprinted PG shows ~10% mismatch [Figs. 3(c) and 3(d)]. This could be related to the non-uniform retardance value across the PG. Averaged phase retardation of

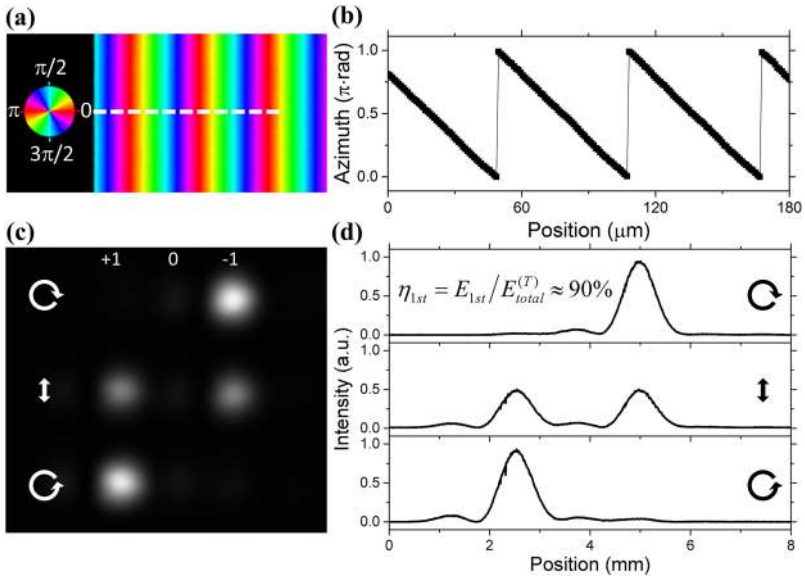

FIG. 3. Femtosecond laser direct writing of the geometric-phase optical element designed as a blazed polarization grating (PG) with a period of 60 μm. (a) Azimuth image of the slow-axis of the imprinted nanogratings; (b) the profile [white dashed line in 3(a)] of azimuth of the slow-axis extracted from the birefringence image. Pseudo colours (inset) indicate the local orientation of the slow-axis. The birefringence measurement system was operating at 546 nm wavelength. (c) Frequency-doubled Nd:YAG cw laser beam profiles of the transmitted right-handed circular (top), linear (middle), and left-handed circular (bottom) polarizations, and (d) its corresponding intensity profiles with the estimated first order diffraction efficiency. White and black arrows indicate the polarization state of the incident and PG transmitted beams.

the printed element with the corresponding azimuth density possesses the relative standard deviation of around 7%–10% [Fig. 1(c)]. Also, the light wave propagating through the large thickness of the structure, i.e., from several microns to tens of microns, could be detuned, and an additional alignment of the geometry of stacked layers should be performed.[43] Roughly 90% of the transmitted light is projected to the ±1st order and 10% to the 0th and higher orders [Fig. 3(d)]. As the handedness of the diffracted circularly polarized beam is flipped, the polarization filtering could be applied in order to completely eliminate the non-diffracted light.

High-precision translation and rotation stages synchronized with the laser system enable the complex designs of geometric phase elements such as computer generated Fourier holograms (CGHs) that convert the initial Gaussian beam into the target intensity distribution. Using the adapted weighted Gerchberg-Saxton algorithm,[44,45] the 8-bit grayscale CGH element with 0.1 megapixel and a pixel spacing of 1.2 μm was designed to encode the Queen Elizabeth II portrait (Fig. 4). During the continuous writing process, the maximum relative phase change of 0.8π between the two adjacent pixels was achieved. By using the Fourier transforming properties of a positive lens, the target image was reconstructed within the spectral range of 450–950 nm [Figs. 4(c)–4(f)]. As it was discussed before, to attain the high-efficiency of an imprinted GP element, the half-wave retardation must be ensured. However, even if the retardance is below this value, the non-diffracted beam can be completely removed by the means of polarization filtering [Fig. 4(a)]. In addition, the geometric phase is independent of wavelength. Therefore, the phase profile for different wavelengths transmitted through the same design will not differ. In this case, the broadband sources can be implemented with a polarization filtering efficiency as high as ~100%.

High-efficiency and independence of wavelength make GP elements attractive for many application areas. For example, taking advantage of the sub-micron resolution of ultrafast laser direct writing, vortex half-wave retarders for optical micro-manipulation can be designed.[46] The vortex half-wave retarder, also referred to as a polarization converter, which transforms the incident linear or circular polarization into radial/azimuthal polarization or optical vortex, respectively, was branded as S-wave plate, patented, and successfully commercialized several years ago.[7,47] We extend the technology and demonstrate the generation of optical vortices with a topological charge of $l = \pm 100$ (Fig. 5). Such

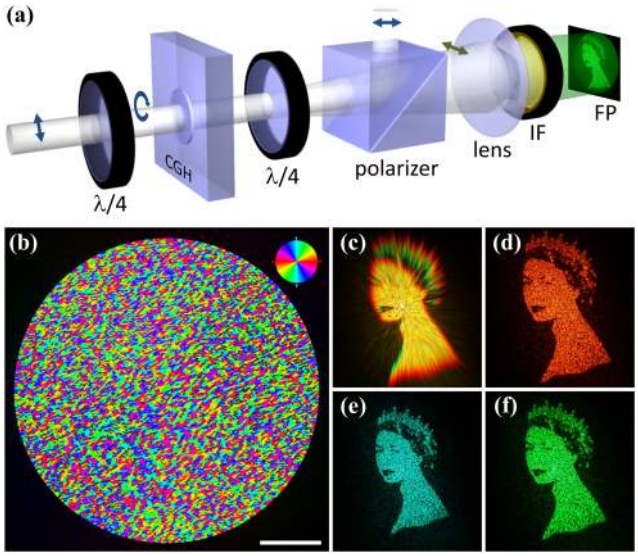

FIG. 4. Computer generated geometric-phase Fourier hologram (CGH). (a) Setup for polarization filtering and target image reconstruction: quarter-wave plates (λ/4), laser imprinted 8-bit grayscale CGH, linear polarizer, lens with f = 50 mm, interference filter (IF), Fourier plane (FP). Arrows indicate the state of beam polarization. (b) Orientation of the slow-axis of laser-imprinted CGH, and [4(c)–4(f)] its resulting reconstructed images. Pseudo colours (inset) indicate the local orientation of the slow-axis. The birefringence measurement system was operating at 546 nm wavelength. The hologram was illuminated with [4(c)–4(f)] a supercontinuum laser beam, where (c) 450-950 nm, (d) 600 nm, (e) 500 nm, and (f) 550 nm filtered wavelengths. Scale bar is 500 μm.

elements with the damage threshold being as high as $\mathrm{LIDT}_{1\text{-on-}1}$ = 26.25 ± 3.15 J/cm^2 (1064 nm, 3.5 ns, 10 Hz)[47] enable the simultaneous optical manipulation of a large number of micro-objects using high-power laser beams.

The electric field of the linearly or elliptically polarized light can be expressed as the superposition of left- and right-handed circular polarizations. Each photon of circularly polarized light carries a spin angular momentum of $S = s\hbar$, where $s = \pm 1$. If these photons are transmitted through the vortex half-wave retarder, the incident spin momentum of S_{in} is changed to $-S_{\mathrm{in}}$, and the orbital momentum L is transferred to the light. So, the total angular momentum is contributed by an orbital angular momentum (OAM) with $L = l\hbar$, where l is an integer number (positive or negative). At the output of the retarder, vortices with the two states of opposite handedness circular polarizations and opposite handedness helical phases are generated. Then, the overall state of the beam corresponds to the amplitude ratio of the incident states with the opposite handedness circular polarizations, which can be continuously controlled by the quarter-wave plate. As a result, the retarder generates a circularly polarized vortex beam with the averaged OAM per photon that is controlled by the angle (θ) of the quarter-wave plate,

$$\langle L(\theta)\rangle = c \cdot \langle S(\theta)\rangle = c \cdot \sin(2\theta)\,\hbar, \tag{2}$$

where c is the integer number referred to as a topological charge of the vortex half-wave retarder (corresponds to $q = c/2$), indicating the number of twists in the azimuth of slow-axis by π within the rotation of the polar angle by $\psi = 2\pi$, with the sign determined by the geometry of the retarder. If the beam with a helical phase of $\phi = l\psi$ possesses well-defined OAM with $l\hbar$,[48] then the l can be shown as $l = cs$, where s is an averaged spin per photon.

Here we demonstrate the printed vortex half-wave retarder with $c = -100$ [Fig. 5(a)]. The retarder is set to have the same topological charge along its radius; thus the azimuth density increases very quickly when the radius is approaching the central point. As a consequence, the relative retardance drops (Fig. 1). Therefore, the center of the element has not been printed, and the incident annular vortex beam ($l = \pm 2$) was used to ensure the uniformity of the phase conversion [Fig. 5(b)]. By continuously rotating the quarter-wave, the ring-shaped beams with total OAM from $\langle L\rangle = -98\hbar$ to $\langle L\rangle = +98\hbar$ were generated [Fig. 5(c)]. Thus, the continuous control of torque without altering the

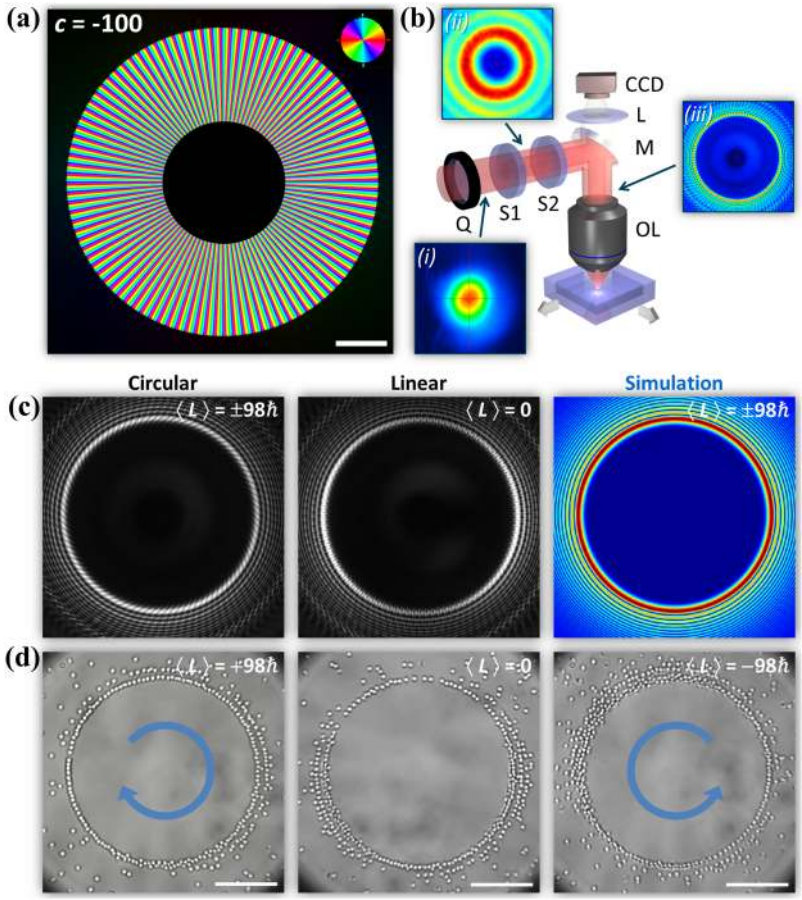

FIG. 5. Single beam optical vortex tweezers with the continuous control of orbital angular momentum (OAM), where any value from $-98\hbar$ to $+98\hbar$ defined by the angle of the quarter-wave plate can be achieved. (a) Geometric-phase based optical vortex retarder with a topological charge of $c = -100$. Scale bar is 1 mm; the color bar indicates the orientation of the slow-axis. The birefringence measurement system was operating at 546 nm wavelength. (b) Optical trapping setup. Inset images show the beam profiles measured at the pupil plane of objective lens (OL): (i) after the quarter-wave plate (Q), (ii) after the Q and vortex retarder (S1) with a topological charge of $c = -2$, and (iii) after the Q, S1, vortex retarder (S2) with a topological charge of $c = -100$, and dichroic mirror (M). Micro-manipulation was monitored by projecting the live images via a focusing lens (L) on a camera detector (CCD). The trapping setup was tuned for the Nd:YVO_4 laser system operating at 1064 nm. (c) Beam intensity distribution measured and simulated at the objective's pupil plane, when the circularly (left and right images) or linearly (middle image) polarized incident Gaussian beam is transmitted through the optical trapping setup. (d) The focused (0.65 NA) vortex beams with OAM varying from $\langle L\rangle = -98\hbar$ to $\langle L\rangle = +98\hbar$ were used to trap and rotate SiO_2 beads (size of 1 μm). Scale bar is 20 μm.

intensity distribution was implemented in optical trapping demonstration with the total 5 W average laser power [Fig. 5(d)], which would not be possible with alternative beam shaping devices.

CONCLUSIONS

The demonstration of high-performance geometric phase elements imprinted in silica glass by the direct-write ultrafast laser nanostructuring shows the potential of technique for designing functional devices that can be integrated into the systems such as high-power lasers, high-resolution microscopy, optical communication systems, polarization sensitive imaging, and consumer electronics. The key advantages such as durability and technological flexibility realizing elements inside transparent solids make the technology exceptional and free of alternatives. Providing high efficiency with low transmission losses and high thermal/chemical stability, the printing of multi-layered optical components with different phase profiles embedded in a single slab of silica glass or fiber could

enable portable/handheld instruments for many practical applications such as endoscopes, integrated miniature illumination, and detection systems.

MATERIALS AND METHODS

The ultrafast laser nanostructuring experiments were carried out with a ytterbium doped potassium gadolinium tungstate (Yb:KGW) based mode-locked regenerative amplified femtosecond laser system PHAROS (Light Conversion Ltd.) operating at a wavelength of 1030 nm with the pulse duration tuned in the range of 300-600 fs. The laser beam was focused with a 0.16 NA–1.2 NA objective lens 300 μm below the surface of a fused silica substrate, which was mounted on a XYZ linear air-bearing translation stage (Aerotech Ltd.). Laser repetition rate and sample translation speed varied from 20 kHz to 200 kHz and 0.02 mm/s to 2 mm/s ensuring the pulse density higher than 1×10^5 pulses/mm. Multiple layers of scanned lines with the interline distance of 1 μm using fixed pulse energy were imprinted in order to achieve the target phase retardation. The pulse energies used in experiments were kept below 2 μJ.

The imprinted elements were optically characterized with the VIS/NIR micro-spectrometer CRAIC (integrated in Olympus BX51) and the quantitative birefringence measurement system CRi Abrio (integrated in Olympus BX51) operating at 546 nm wavelength. An Nd:YAG cw laser (Spectra-Physics) frequency-doubled to 532 nm and a supercontinuum fiber laser (Fianium) emitting a broad optical spectrum in the range of 450–950 nm were used to probe the Gaussian beam propagation through the imprinted GP elements. Optical trapping experiments were performed with an Nd:YVO_4 picosecond laser system (Rapid, Coherent, Inc.) operating at a wavelength of 1064 nm with the pulse duration of 10 ps and repetition rate of 640 kHz (burst of 31 pulses with 50 MHz). Imaging of laser-induced nanogratings was performed with a scanning electron microscope (Zeiss Evo50), after the characteristic topography was revealed during the lapping/polishing and KOH (1 mol/l) etching procedures.

ACKNOWLEDGMENTS

The study has been supported by EPSRC (Grant No. EP/M029042/1) and the Ministry of Education and Science of Russia (Grant No. 14.Z50.31.0009). The data for this work are accessible through the University of Southampton Institutional Research Repository (dx.doi.org/10.5258/SOTON/400343).

[1] N. Yu and F. Capasso, "Flat optics with designer metasurfaces," Nat. Mater. **13**, 139–150 (2014).
[2] M. Khorasaninejad, W. T. Chen, R. C. Devlin, J. Oh, A. Y. Zhu, and F. Capasso, "Metalenses at visible wavelengths: Diffraction-limited focusing and subwavelength resolution imaging," Science **352**(6290), 1190–1194 (2016).
[3] X. Ni, N. K. Emani, A. V. Kildishev, A. Boltasseva, and V. M. Shalaev, "Broadband light bending with plasmonic nanoantennas," Science **335**, 427 (2011).
[4] N. Yu, P. Genevet, M. A. Kats, F. Aieta, J.-P. Tetienne, F. Capasso, and Z. Gaburro, "Light propagation with phase discontinuities reflection and refraction," Science **334**, 333–337 (2011).
[5] Z. Bomzon, G. Biener, V. Kleiner, and E. Hasman, "Space-variant Pancharatnam-Berry phase optical elements with computer-generated subwavelength gratings," Opt. Lett. **27**(13), 1141–1143 (2002).
[6] M. N. Miskiewicz and M. J. Escuti, "Direct-writing of complex liquid crystal patterns," Opt. Express **22**(10), 12691–12706 (2014).
[7] M. Beresna, M. Gecevičius, and P. G. Kazansky, "Polarization sensitive elements fabricated by femtosecond laser nanostructuring of glass," Opt. Mater. Express **1**(4), 783–795 (2011).
[8] D. Lin, P. Fan, E. Hasman, and M. L. Brongersma, "Dielectric gradient metasurface optical elements," Science **345**(6194), 298–302 (2014).
[9] S. Jahani and Z. Jacob, "All-dielectric metamaterials," Nat. Nanotechnol. **11**(1), 23–36 (2016).
[10] B. Y. S. Pancharatnam, "Generalized theory of interference, and its applications. Part I. Coherent pencils," Proc. Indian Acad. Sci. A **44**, 247–262 (1956).
[11] M. V. Berry, "Quantal phase factors accompanying adiabatic changes," Proc. R. Soc. London, Ser. A **392**, 45–57 (1984).
[12] J. Anandan, "The geometric phase," Nature **360**, 307–313 (1992).
[13] Z. Bomzon, V. Kleiner, and E. Hasman, "Pancharatnam-Berry phase in space-variant polarization-state manipulations with subwavelength gratings," Opt. Lett. **26**(18), 1424–1426 (2001).
[14] N. Meinzer, W. L. Barnes, and I. R. Hooper, "Plasmonic meta-atoms and metasurfaces," Nat. Photonics **8**(12), 889–898 (2014).

[15] G. Zheng, H. Mühlenbernd, M. Kenney, G. Li, T. Zentgraf, and S. Zhang, "Metasurface holograms reaching 80% efficiency," Nat. Nanotechnol. **10**, 308–312 (2015).
[16] J. Kim, Y. Li, M. N. Miskiewicz, C. Oh, M. W. Kudenov, and M. J. Escuti, "Fabrication of ideal geometric-phase holograms with arbitrary wavefronts," Optica **2**(11), 958 (2015).
[17] P. F. McManamon, P. J. Bos, M. J. Escuti, J. Heikenfeld, S. Serati, H. Xie, and E. A. Watson, "A review of phased array steering for narrow-band electrooptical systems," Proc. IEEE **97**(6), 1078 (2009).
[18] L. Marrucci, C. Manzo, and D. Paparo, "Pancharatnam-Berry phase optical elements for wave front shaping in the visible domain: Switchable helical mode generation," Appl. Phys. Lett. **88**(22), 221102 (2006).
[19] S. K. Sundaram and E. Mazur, "Inducing and probing non-thermal transitions in semiconductors using femtosecond laser pulses," Nat. Mater. **1**, 217–224 (2002).
[20] R. R. Gattass and E. Mazur, "Femtosecond laser micromachining in transparent materials," Nat. Photonics **2**, 219–225 (2008).
[21] Y. Shimotsuma, P. Kazansky, J. Qiu, and K. Hirao, "Self-organized nanogratings in glass irradiated by ultrashort light pulses," Phys. Rev. Lett. **91**(24), 247405 (2003).
[22] P. Kazansky, H. Inouye, T. Mitsuyu, K. Miura, J. Qiu, K. Hirao, and F. Starrost, "Anomalous anisotropic light scattering in Ge-doped silica glass," Phys. Rev. Lett. **82**(10), 2199–2202 (1999).
[23] V. Bhardwaj, E. Simova, P. Rajeev, C. Hnatovsky, R. Taylor, D. Rayner, and P. Corkum, "Optically produced arrays of planar nanostructures inside fused silica," Phys. Rev. Lett. **96**(5), 057404 (2006).
[24] M. Beresna, M. Gecevičius, P. G. Kazansky, T. Taylor, and A. V. Kavokin, "Exciton mediated self-organization in glass driven by ultrashort light pulses," Appl. Phys. Lett. **101**(5), 053120 (2012).
[25] F. Liang, R. Vallée, and S. Chin, "Physical evolution of nanograting inscription on the surface of fused silica," Opt. Mater. Express **2**(7), 900–906 (2012).
[26] Y. Liao, J. Ni, L. Qiao, M. Huang, Y. Bellouard, K. Sugioka, and Y. Cheng, "High-fidelity visualization of formation of volume nanogratings in porous glass by femtosecond laser irradiation," Optica **2**(4), 329 (2015).
[27] F. Zimmermann, A. Plech, S. Richter, A. Tünnermann, and S. Nolte, "The onset of ultrashort pulse-induced nanogratings," Laser Photonics Rev. **10**, 327–334 (2016).
[28] A. Rudenko, J.-P. Colombier, and T. E. Itina, "From random inhomogeneities to periodic nanostructures induced in bulk silica by ultrashort laser," Phys. Rev. B **93**(7), 075427 (2016).
[29] R. Taylor, C. Hnatovsky, and E. Simova, "Applications of femtosecond laser induced self-organized planar nanocracks inside fused silica glass," Laser Photonics Rev. **2**(1–2), 26–46 (2008).
[30] M. Lancry, B. Poumellec, J. Canning, K. Cook, J.-C. Paulin, and F. Brisset, "Ultrafast nanoporous silica formation driven by femtosecond laser irradiation," Laser Photonics Rev. **7**(6), 953–962 (2013).
[31] V. Oliveira, S. P. Sharma, P. Herrero, and R. Vilar, "Transformations induced in bulk amorphous silica by ultrafast laser direct writing," Opt. Lett. **38**(23), 4950–4953 (2013).
[32] E. Bricchi and P. G. Kazansky, "Extraordinary stability of anisotropic femtosecond direct-written structures embedded in silica glass," Appl. Phys. Lett. **88**(11), 111119 (2006).
[33] E. Bricchi, J. D. Mills, P. G. Kazansky, B. G. Klappauf, and J. J. Baumberg, "Birefringent Fresnel zone plates in silica fabricated by femtosecond laser machining," Opt. Lett. **27**(24), 2200 (2002).
[34] W. Cai, T. J. Reber, and R. Piestun, "Computer-generated volume holograms fabricated by femtosecond laser micromachining," Opt. Lett. **31**(12), 1836–1838 (2006).
[35] D. Papazoglou and M. Loulakis, "Embedded birefringent computer-generated holograms fabricated by femtosecond laser pulses," Opt. Lett. **31**(10), 1441–1443 (2006).
[36] Y. Li, Y. Dou, R. An, H. Yang, and Q. Gong, "Permanent computer-generated holograms embedded in silica glass by femtosecond laser pulses," Opt. Express **13**(7), 2433–2438 (2005).
[37] W. Cai, A. Libertun, and R. Piestun, "Polarization selective computer-generated holograms realized in glass by femtosecond laser induced nanogratings," Opt. Express **14**(9), 3785–3791 (2006).
[38] R. Berlich, D. Richter, M. Richardson, and S. Nolte, "Fabrication of computer-generated holograms using femtosecond laser direct writing," Opt. Lett. **41**(8), 1752 (2016).
[39] M. Gecevičius, M. Beresna, R. Drevinskas, and P. G. Kazansky, "Airy beams generated by ultrafast laser-imprinted space-variant nanostructures in glass," Opt. Lett. **39**(24), 6791–6794 (2014).
[40] R. Desmarchelier, M. Lancry, M. Gecevicius, M. Beresna, P. G. Kazansky, and B. Poumellec, "Achromatic polarization rotator imprinted by ultrafast laser nanostructuring in glass," Appl. Phys. Lett. **107**, 181111 (2015).
[41] R. Drevinskas, M. Beresna, J. Zhang, A. G. Kazanskii, and P. G. Kazansky, "Ultrafast laser-induced metasurfaces for geometric phase manipulation," Adv. Opt. Mater. **5**(1), 1600575 (2017).
[42] E. Hasman, Z. Bomzon, A. Niv, G. Biener, and V. Kleiner, "Polarization beam-splitters and optical switches based on space-variant computer-generated subwavelength quasi-periodic structures," Opt. Commun. **209**, 45–54 (2002).
[43] M. L. Ng, D. Chanda, and P. R. Herman, "Coherent stitching of light in multilayered diffractive optical elements," Opt. Express **20**(21), 23960 (2012).
[44] R. Di Leonardo, F. Ianni, and G. Ruocco, "Computer generation of optimal holograms for optical trap arrays," Opt. Express **15**(4), 1913–1922 (2007).
[45] J. Zhang, M. Gecevičius, M. Beresna, and P. G. Kazansky, "Seemingly unlimited lifetime data storage in nanostructured glass," Phys. Rev. Lett. **112**(3), 033901 (2014).
[46] M. Gecevičius, R. Drevinskas, M. Beresna, and P. G. Kazansky, "Single beam optical vortex tweezers with tunable orbital angular momentum," Appl. Phys. Lett. **104**(23), 231110 (2014).
[47] See http://www.altechna.com/product_details.php?id=1048 for Altechna. S-waveplate (Radial Polarization Converter).
[48] L. Allen, M. W. Beikersbergen, R. J. C. Spreeuw, and J. P. Woerdman, "Orbital angular momentum of light and the transformation of Laguerre-Gaussian laser modes," Phys. Rev. A **45**(11), 8185–8189 (1992).